Interactions of Intermediate Semiquinone with Surrounding Protein Residues at the Q(H) Site of Wild-Type and D75H Mutant Cytochrome bo(3) from Escherichia coli

ARTICLE *in* BIOCHEMISTRY · APRIL 2012

Impact Factor: 3.02 · DOI: 10.1021/bi300151q · Source: PubMed

10 AUTHORS, INCLUDING:

Rimma I Samoilova
Russian Academy of Sciences
78 PUBLICATIONS **873** CITATIONS
SEE PROFILE

Kv Narasimhulu
Tampa, USA
46 PUBLICATIONS **892** CITATIONS
SEE PROFILE

Patrick J O'Malley
The University of Manchester
47 PUBLICATIONS **707** CITATIONS
SEE PROFILE

Robert B Gennis
University of Illinois, Urbana-Champaign
371 PUBLICATIONS **12,649** CITATIONS
SEE PROFILE

Published in final edited form as:
Biochemistry. 2012 May 8; 51(18): 3827–3838. doi:10.1021/bi300151q.

Interactions of intermediate semiquinone with surrounding protein residues at the Q_H site of the wild-type and D75H mutant cytochrome *bo*$_3$ from *Escherichia coli*†

Myat T. Lin[⊥,1], **Amgalanbaatar Baldansuren**[¶], **Richard Hart**[#], **Rimma I. Samoilova**[§], **Kuppala V. Narasimhulu**[¶], **Lai Lai Yap**[‡], **Sylvia K. Choi**[⊥], **Patrick J. O'Malley**[#,*], **Robert B. Gennis**[⊥,‡,*], and **Sergei A. Dikanov**[¶,*]

[⊥]Center for Biophysics & Computational Biology, University of Illinois at Urbana-Champaign, Urbana, Illinois 61801

[‡]Department of Biochemistry, University of Illinois at Urbana-Champaign, Urbana, Illinois 61801

[¶]Department of Veterinary Clinical Medicine, University of Illinois at Urbana-Champaign, Urbana, Illinois 61801

[§]Institute of Chemical Kinetics and Combustion, Russian Academy of Sciences, Novosibirsk 630090, Russia

[#]School of Chemistry, The University of Manchester, Manchester M13 9PL, UK

Abstract

Selective ^{15}N isotope labeling of the cytochrome *bo*$_3$ ubiquinol oxidase from *E. coli* with auxotrophs was used to characterize the hyperfine couplings with the side-chain nitrogens from R71, H98, and Q101 residues and peptide nitrogens from R71 and H98 residues around the semiquinone (SQ) at the high-affinity Q_H site. The 2D ESEEM (HYSCORE) data have directly identified the N_ε of R71 as an H-bond donor carrying the largest amount of the unpaired spin density. In addition, weaker hyperfine couplings with the side-chain nitrogens from all residues around the SQ were determined. These hyperfine couplings reflect a distribution of the unpaired spin density over the protein in the SQ state of the Q_H site and strength of interaction with different residues. The approach was extended to the virtually inactive D75H mutant, where the intermediate SQ is also stabilized. We found that the N_ε from a histidine residue, presumably H75, carries most of the unpaired spin density instead of the N_ε of R71, as in the wild-type *bo*$_3$. However, the detailed characterization of the weakly coupled ^{15}Ns from selective labeling of R71 and Q101 in D75H was precluded by overlap of the ^{15}N lines with the much stronger ~1.6 MHz line from quadrupole triplet of the strongly coupled $^{14}N_\varepsilon$ from H75. Therefore, a reverse labeling approach, in which the enzyme was uniformly labeled except for selected amino acid types, was applied in order to probe the contribution of R71 and Q101 to the ^{15}N signals. Such labeling has shown only weak coupling with all nitrogens of R71 and Q101. We utilize density functional theory based calculations to model the available information about ^{1}H, ^{15}N and ^{13}C hyperfine

†This investigation was supported by the DE-FG02-08ER15960 (S.A.D.) and DE-FG02-87ER13716 (R.B.G.) Grants from Chemical Sciences, Geosciences and Biosciences Division, Office of Basic Energy Sciences, Office of Sciences, US DOE, and the NIH GM062954 Grant (S.A.D) and NCRR/NIH Grants S10-RR015878 and S10-RR025438 for instrumentation.

*Corresponding Author S.A.D.: dikanov@illinois.edu; phone, +1 217 333 3776. R.B.G.: r-gennis@illinois.edu; phone, +1 217 333 9075. P.J.O.M.: patrick.o'malley@manchester.ac.uk; phone, +44 161 306 4536l.
[1]Present address: 321 Biotechnology Building, Department of Molecular Biology and Genetic, Cornell University, Ithaca, NY 14853

Supporting Information Available: model of the Q_H-site, ^{14}N,^{15}N three-pulse and HYSCORE spectra of the Q_H site SQ in WT and D75H cyt *bo*$_3$, the structures of amino acids selectively labeled in this work showing the atomic numberings, complete ref. 27. This material is available free of charge via the Internet at http://pubs.acs.org.

couplings for the Q_H site and to describe the protein-substrate interactions in both enzymes. In particular, we identify the factors responsible for the asymmetric distribution of the unpaired spin density and ponder the significance of this asymmetry to the quinone's electron transfer function.

Cytochrome *bo*$_3$ ubiquinol oxidase (cyt *bo*$_3$) from *Escherichia coli* catalyzes the reduction of molecular oxygen to water using ubiquinol as the electron donor.[1] The enzyme located in the cytoplasmic membrane also functions as a proton pump, conserving much of the energy available from the redox reaction as the proton motive force.[2,3] Cyt *bo*$_3$ is a member of heme-copper superfamily. Of the four subunits of cyt *bo*$_3$, the catalytic subunit and two other subunits are analogous to the mitochondrially encoded subunits of *aa*$_3$-type cytochrome *c* oxidase (cyt *aa*$_3$).[4] Despite having different electron donors, the proton pumps of cyt *bo*$_3$ and cyt *aa*$_3$ likely operate in a similar manner.[5]

Previous work has established that cyt *bo*$_3$ isolated in the detergent n-dodecyl β-D-maltoside (DDM) is associated with a tightly bound ubiquinone-8 (UQ_8) at the Q_H site, whereas purification in Triton X-100 yields the enzyme without any bound UQ_8.[6,7] The UQ_8 bound at the Q_H site does not exchange with the substrate ubiquinone pool during turnover. Hence, the Q_H site is distinct from the Q_L site, where the oxidation of substrate ubiquinol takes place.[7,8] The Q_H site has been shown to be able to stabilize the one-electron reduced semiquinone (SQ_H), which can be detected by EPR spectroscopy.[9,10] The comparison of the kinetics between the enzyme preparations with and without the tightly bound UQ_8 or with the Q_H site inhibitors led to the conclusion that the UQ_8 at the Q_H site facilitates the fast electron transfer process from the substrate ubiquinol to the low spin heme *b*.[6,11–13]

A crystal structure of cyt *bo*$_3$ without a bound UQ_8 has been reported.[14] Based on the crystal structure and mutagenesis studies, residues R71, D75, H98 and Q101 from subunit I were proposed to interact with the bound UQ_8 at the Q_H site (Fig. 1).[14,15] Mutating any of the four residues led to the loss of catalytic activity. Notably, the D75H mutant, despite its inability to reduce molecular oxygen, was found to stabilize a SQ radical with a midpoint potential similar to that of the wild type (WT) enzyme.[15] Hence, an environment resulting in the stabilization of the SQ radical is necessary but not sufficient for proper function. A precise spatial arrangement of the SQ radical and the surrounding residues at the Q_H site is crucial for the successful electron transfer process.

Previous X-band 1D and 2D ESEEM experiments have offered insights into the nature of interactions between the SQ_H and the Q_H site residues (Fig. 1).[16–20] Hyperfine couplings with methyl group protons and exchangeable, hydrogen bonded protons, are consistent with a neutral SQ_H species in the WT cyt *bo*$_3$, indicating significant asymmetry in the distribution of the unpaired spin density.[17] The ^{14}N ESEEM spectra reveal one strongly coupled nitrogen participating in a hydrogen bond with the SQ_H.[16–18] In a previous communication, we reported selective ^{15}N-labeling of cyt *bo*$_3$, identifying the N_ε of R71 as the strongly coupled nitrogen in the WT cyt *bo*$_3$ and have shown that the other nitrogens in R71, H98 and Q101 possess substantially smaller couplings.[19] In contrast, a strongly coupled nitrogen that is observed in the ^{14}N ESEEM spectra of the SQ_H radical of the inactive D75H mutant was shown to be from a different amino acid residue.[18] The SQ_H is stabilized by hydrogen bonds different from the ones identified with the WT enzyme and its characteristics are shifted towards an anion-radical.

In the current work we provide the comparative analysis of the 2D ESEEM (HYSCORE) spectra of ^{15}N uniformly labeled (^{15}N-U) WT and D75H cyt *bo*$_3$. We report the complete results of selective ^{15}N-labeling of the residues at the Q_H site in these two enzymes. In addition to the strongly coupled N_ε of R71, the weakly coupled N_ε of H98 was also found to carry unpaired spin density in the WT cyt *bo*$_3$. It is also shown that in the D75H mutant, the

N_ε of H75 is the strongly coupled nitrogen, and the N_ε of R71 displays significantly weaker hyperfine interaction with the SQ_H. The principal values of the rhombic hyperfine tensors for the strongly coupled nitrogens in WT and D75H cyt *bo*$_3$ were determined using a newly developed method of HYSCORE cross-peak lineshape analysis. In addition to ^{15}N couplings from the present work, ^{1}H and ^{13}C couplings from previous studies of the WT and D75H cyt *bo*$_3$[17,18,20] were utilized in QM/MM calculations to calculate the spatial environment and electronic structure of the SQ_H. In particular, these calculations identify the factors responsible for the asymmetric distribution of the unpaired spin density and charge at the Q_H site and ponder the significance of this asymmetry to the quinone's electron transfer function.

Materials and Methods

Materials

Isopropyl-β-D-thiogalactopyranoside (IPTG) was bought from Fisher Scientific (Pittsburgh, PA). n-dodecyl-β-D-maltoside (DDM) was purchased from Anatrace (Maumee, OH). $^{15}NH_4Cl$ and ^{15}N-enriched amino acids for the growth of *E. coli* to express isotope labeled cyt *bo*$_3$ were ordered from Cambridge Isotope Laboratories (Andover, MA). Other chemicals used in the preparation of growth medium and buffers were from Sigma-Aldrich (St. Louis, MO).

Bacterial Strains

E. coli C43(DE3) strains with deletions of genes involved in amino-acid biosynthetic pathways were constructed with the λ-Red recombination system as described previously.[20,21] The C43(DE3) auxotroph strains used in the current work are listed in Table 1.

Preparation of Amino-acid Selective Isotope Labeled Cyt bo$_3$

Selectively ^{15}N labeled cyt *bo*$_3$ samples were expressed from the various C43(DE3) auxotroph strains as summarized in Table 1. Each auxotroph to be used as an expression host was transformed with the pET-17b vector (Novagen) encoding the WT or D75H mutant cyo operon engineered to encode cyt *bo*$_3$ with a 6xHis tag at the C terminus of subunit II.[18] The enzymes overexpressed from the C43(DE3) cultures were solublized in DDM detergent, purified with Ni-NTA affinity chromatography and reduced with sodium ascorbate under anaerobic condition to generate the SQ_H radical as described previously.[20]

EPR Measurements

The CW EPR measurements were performed on an X-band Varian EPR-E122 spectrometer. The pulsed EPR experiments were carried out using an X-band Bruker ELEXSYS E580 spectrometer equipped with Oxford CF 935 cryostats. Unless otherwise indicated, all measurements were made at 50 K. Some pulsed EPR measurements were also performed at higher temperatures, up to 120 K, and the results were similar to those obtained at 50 K. Several types of ESE experiments with different pulse sequences were employed with appropriate phase cycling schemes to eliminate unwanted features from the experimental echo envelopes. Among them are two-dimensional three-pulse and four-pulse sequences, which are described in detail elsewhere.[17] Spectral processing of three- and four-pulse ESEEM patterns, including subtraction of relaxation decay (fitting by 3–6 degree polynomials), apodization (Hamming window), zero filling, and fast Fourier transformation, was performed using Bruker WIN-EPR software.

Some HYSCORE spectra are presented as contour plots in Matlab R14. For the 2D data representation, the echo decay was eliminated by low-order polynomial (up to fourth-order)

base-line corrections in each dimension and apodizied with a Hamming window subsequently. Before the 2D Fourier transformation, the data was zero-filled up to a 1024 × 1024 matrix. The evaluated values were subsequently used to simulate the 2D HYSCORE spectra applying the Kazan Viewer package[22] or home written PC software developed by Dr. A. Tyryshkin (now at Princeton University).[23]

HYSCORE Spectra from ^{15}N Nuclei

The experimental data regarding the ligand environment of the semiquinone were obtained in this work from the two-dimensional (2D) ^{15}N ESEEM (HYSCORE) spectra.[24] The HYSCORE technique creates 2D spectra with off-diagonal cross-peaks. ^{15}N nucleus with I=1/2 has two hyperfine frequencies ν_α and ν_β from opposite m_s=±1/2 electron spin manifolds. These may produce a pair of cross-features (ν_α, ν_β) and (ν_β, ν_α) in (++) quadrant, as well as another pair ($-\nu_\alpha$, ν_β) and (ν_α, $-\nu_\beta$) in the (+−) quadrant. The appearance of cross-peaks in (++) or (+−) quadrants is governed by the relative values of hyperfine couplings ^{15}A and Zeeman frequency $^{15}\nu_N$.[25,26] Peaks in the (+−) quadrant come primarily from strong hyperfine interaction, i.e. $|^{15}A|>2(^{15}\nu_N)$, whereas the peaks in the (++) quadrant appear predominantly from interactions with $|^{15}A|<2(^{15}\nu_N)$. Peaks may appear in both quadrants simultaneously in the intermediate case when both parts of the inequalities are comparable.

Orientation-disordered (*i.e.* powder) 2D spectra of I=1/2 nuclei also reveal, in the form of cross-ridges contour projections, the interdependence between ν_α and ν_β values in the same orientation. The two coordinates of the arbitrary point at the cross-ridge, described in the first order by equation

$$\nu_{\alpha(\beta)}=|^{15}\nu_N+(-)|^{15}A|/2| \quad (1)$$

can be used for the first-order estimate of the corresponding hyperfine coupling constant A:

$$\begin{aligned} \nu_\alpha-\nu_\beta&=|A| \text{ if } |^{15}A|<2(^{15}\nu_N) \\ \nu_\alpha+\nu_\beta&=|A| \text{ if } |^{15}A|>2(^{15}\nu_N) \end{aligned} \quad (2)$$

On the other hand, analysis of the cross-ridges in $(\nu_\alpha)^2$ *vs.* $(\nu_\beta)^2$ coordinates and spectral simulations allows in many cases for simultaneous determination of the isotropic a_{iso} and anisotropic T components of the hyperfine tensor.[25,26]

Computational methods

All density functional calculations were performed using Gaussian 09.[27] All calculations including geometry optimization and hyperfine coupling were performed using the B3LYP functional and the EPR-II basis set. Specific details concerning hyperfine coupling calculations are as previously described.[28,29] Details of specific models used are given in the text.

Results and discussion

^{14}N and ^{15}N ESEEM spectra of Wild Type and D75H Mutant of Cyt bo$_3$

The interaction of the SQ_H with the protein environment in WT and D75H cyt bo_3 with natural abundance of nitrogen (^{14}N isotope - 99.63 %) has been previously studied in detail by pulsed EPR spectroscopy.[16–18] 1D and 2D ^{14}N ESEEM spectra show the contribution from only a single nitrogen in each protein (Figs. S1 and S2). These possess different characteristics, i.e. quadrupole coupling constant (qcc) K=0.93 MHz, asymmetry parameter η=0.51, and hyperfine coupling ^{14}A=1.8 MHz for WT cyt bo_3[16,17] and K=0.43 MHz, η

=0.73, and ^{14}A=2.7 MHz for D75H.[18] The values of K and η characterize the chemical type and electronic configuration of ^{14}N atom interacting with the SQ_H. For instance, $K=e^2qQ/4h$=0.93 MHz, most closely corresponds to the nitrogen from an NH or NH_2 group.[17,18] This value is ~10% larger than the qcc for the peptide amide nitrogen and more than two times the qcc of the protonated imidazole nitrogens in histidine. Therefore, it was suggested that the most likely candidates for the H-bond donor in WT cyt *bo*$_3$ are the nitrogens from the side chains of R71 or Q101. Likewise, a protonated imidazole nitrogen of a histidine residue H75 or H98 was suggested as the H-bond donor in the D75H mutant.[18] ^{14}N spectra do not show any lines from other side-chain and peptide nitrogens of the nearby environment. These nitrogens are coupled more weakly and do not produce well defined lines in the ^{14}N powder-type spectra, because of the nuclear quadrupole interactions (nqi) influence.[30,31] In contrast, the lines from weakly coupled nitrogens (**N_{wc}**) are well observed in 2D ^{15}N ESEEM spectra, which are not complicated by nqi.

Two presentations of ^{15}N HYSCORE spectrum of the SQ_H in ^{15}N-U WT cyt *bo*$_3$ are shown in Fig. 2A,C (see also Fig. S3). The (++) quadrant exhibits a pair of intensive cross-peaks **1** located symmetrically around the diagonal point ($^{15}\nu_N$,$^{15}\nu_N$), along the antidiagonal with maxima at (2.74, 0.34) MHz, which correspond to hyperfine coupling ^{15}A=2.4 MHz. This coupling is in agreement with the expected ^{15}A of 2.5 MHz rescaled from the hyperfine coupling ^{14}A of 1.8 MHz measured from ^{14}N ESEEM spectra. In addition, the (++) quadrant contains feature **N_{wc}** with the maximum near the diagonal point ($^{15}\nu_N$,$^{15}\nu_N$) with the decaying shoulders symmetrically extended up to ~0.8 MHz along the antidiagonal.

The ^{15}N HYSCORE spectrum of the ^{15}N-U D75H mutant (Fig. 2B,D) shows a pair of intensive cross-peaks **1** in the (+−) quadrant with maxima at ~(±3.3, −/+0.4) MHz defining ^{15}A=3.7 MHz or ^{14}A=2.6 MHz, also consistent with the coupling estimated from ^{14}N spectra. The (++) quadrant of the spectrum (Fig. 2B,D) exhibits also **N_{wc}** feature located around the ($^{15}\nu_N$,$^{15}\nu_N$) point. The **N_{wc}** feature in D75H has a different shape compared to that of the WT enzyme. For D75H, the **N_{wc}** feature is a triplet, including a central peak at ($^{15}\nu_N$,$^{15}\nu_N$) and two other lines symmetrically located around the antidiagonal with the splitting ~0.6 MHz.

The ^{14}N and ^{15}N ESEEM spectra show the presence of one strongly coupled nitrogen in the SQ_H environment, which is different in the WT and D75H cyt *bo*$_3$ proteins. In contrast, the **N_{wc}** features resolved in ^{15}N spectra of both the WT and D75H mutant result from *multiple* non-equivalent contributions of weakly-coupled nitrogen nuclei from in the immediate vicinity of the SQ_H. The shapes of the **N_{wc}** features indicate differences in the individual interactions for the SQ_H of the WT and D75H mutant. To further resolve the interactions with nitrogens in the SQ_H environment, selective ^{15}N labeling in different residues, as well as ^{15}N uniform labeling was employed.

Selective ^{15}N labeling of the WT cyt bo_3 protein

Arg, His and Gln were targeted for selective ^{15}N labeling because the corresponding residues are involved in the current model of Q_H-site (Fig. 1). The molecular structure and atomic numbering of each of the three amino acids are displayed in Fig. S4. The following samples of WT cyt *bo*$_3$ were prepared with ^{15}N labels as follows. **1**) Arg: a) uniform labeling; b) the two N_η positions; c) the peptide position N_α; **2**) His: a) uniform labeling; b) ring-^{15}N (N_δ and N_ε); c) the N_δ position only; **3**) Gln with ^{15}N in the N_ε position; **4**) uniformly labeled with ^{15}N except for Arg, Gln and His. It is assumed that only R71, Q101 and H98 are significant in interpreting the interactions with SQ_H.

The following results were obtained.

1. As shown previously, a dramatic change of the ESEEM spectra, accompanied by the complete disappearance of the ^{14}N peaks, is observed with the WT cyt *bo*$_3$ with uniformly ^{15}N-labeled R71 (ref.19, Fig. S5A). The HYSCORE spectrum of the SQ_H in this protein contains two intense cross-peaks **1** similar to ones in the spectrum of ^{15}N-U WT cyt *bo*$_3$ (Fig. 2A,C). In contrast, the $\mathbf{N_{wc}}$ feature observed with ^{15}N-U R71 WT cyt *bo*$_3$ is very different (Fig. S5A), and resolves only a weak doublet centered around the ($^{15}\nu_N$, $^{15}\nu_N$) diagonal point with the splitting ^{15}A=0.15 MHz. A similar doublet was observed in the spectrum of the WT cyt *bo*$_3$ with the selectively labeled $^{15}N_\eta$ ositions in R71 (ref.19, Fig. S5B), whereas no ^{15}N resolved peaks were observed in a sample in which the peptide nitrogen N_α of R71 was selectively labeled with ^{15}N. These observations show a weak interaction in the WT cyt *bo*$_3$ between the SQ_H with the $^{15}N_\eta$ of R71, and confirm that the N_ε of R71 possesses the largest hyperfine coupling and is responsible for the ^{14}N spectral features in the WT cyt *bo*$_3$.

2. It was previously shown that the spectrum of cyt *bo*$_3$ with uniformly ^{15}N-labeled H98 shows the $\mathbf{N_{wc}}$ feature with a maximum at the ($^{15}\nu_N$,$^{15}\nu_N$) point accompanied by extended shoulders up to 0.6 MHz with very poorly resolved maxima.[19] This line can be produced by the interactions with up to three ^{15}Ns and additional selective ^{15}N labeling was performed to clarify the origins of this feature. The spectra of the sample with ring-^{15}N (N_δ and N_ε) labeled His is identical to that with uniformly ^{15}N labeled His (Fig. S5C and Fig. S5D), but a very week antidiagonal ^{15}N line is found in the spectrum of the protein with $^{15}N_\delta$ His. Thus, it is concluded that the extended $^{15}\mathbf{N_{wc}}$ feature is primarily due to the N_ε of H98.

It is noted that a peak of very low intensity located at the diagonal point ($^{15}\nu_N$,$^{15}\nu_N$) was previously observed for the WT cyt *bo*$_3$ with ^{15}N labeled N_ε of Q101, indicating very weak dipolar interaction between the unpaired electron and a distant ^{15}N nucleus.[19] No ^{15}N signal was found in the spectra of WT cyt *bo*$_3$ uniformly labeled with ^{15}N except for Arg, Gln and His. Based on these observations, it is concluded that the only contributions to the $\mathbf{N_{wc}}$ feature are from R71, Q101 and H98.

Selective ^{15}N labeling of D75H

Selectively ^{15}N labeled D75H cyt *bo*$_3$ samples were also examined. The ^{14}N signals completely disappeared in the HYSCORE spectrum of the D75H with uniformly ^{15}N(3)-labeled His (Fig. S6). This result is consistent with the prediction, based on the value of the qcc, that the ^{14}N ESEEM spectrum of the D75H mutant arises from the protonated imidazole ring nitrogen of a histidine residue, presumably either H75 or H98.[18] In order to definitively identify whether the N_δ or N_ε of His contribute to the ^{14}N ESEEM spectra, a D75H with $^{15}N_\delta$ His was prepared. The ^{14}N HYSCORE spectrum of this sample is identical to the spectrum of unlabeled D75H in Fig. S2, so it can be concluded that these spectroscopic features originate from the N_ε of a His residue.

The $\mathbf{N_{wc}}$ feature in the HYSCORE spectrum from the enzyme with uniformly labeled ^{15}N(3) His possesses the maximum intensity at the ($^{15}\nu_N$,$^{15}\nu_N$) diagonal point and shoulders extended up to 0.5 MHz in both directions from the diagonal (Fig. 3B). However, the total intensity of the diagonal peak and shoulders is substantially lower than in the ^{15}N-U enzyme (Fig. 3A), using the cross-peaks **1** as the reference for the intensity comparison. The larger intensity and different shape of the $\mathbf{N_{wc}}$ feature that is only observed in the uniformly labeled ^{15}N-U D75H mutant, must be due to the additional contributions from nitrogens in R71 and Q101 residues.

Unfortunately, the HYSCORE spectra collected from the D75H selectively labeled with ^{15}N Arg or ^{15}N Gln do not resolve the signals from the weakly coupled ^{15}N because any such signal is overshadowed by much more intense peak ν_+ =1.61 MHz from the strongly coupled $^{14}N_\varepsilon$ of His (Fig. S7). In order to visualize the $\mathbf{N_{wc}}$ from R71 and Q101 in the D75H mutant, a reverse labeling approach was employed to prepare ^{15}N-U D75H except for Arg. The contributions of the nitrogen interactions from R71 and Q101 to the ^{15}N spectrum were then obtained using the spectra of (**a**) ^{15}N-U D75H; (**b**) D75H with ^{15}N-His(3); and (**c**) ^{15}N-U D75H with ^{14}N Arg. The subtractions **a–c** and **c–b** give the $\mathbf{^{15}N_{wc}}$ difference spectra from R71 and Q101, respectively (Fig. 3 C,D). The difference spectrum isolating the contribution from R71 shows extended shoulders with the maximum corresponding to the splitting ~0.6 MHz. The difference spectrum showing the contribution from Q101 consists of a weak peak at the diagonal point ($^{15}\nu_N$,$^{15}\nu_N$). In addition we have prepared the ^{15}N-U D75H except for the N_ε and N_α of Arg. The shape of $\mathbf{N_{wc}}$ for this sample is similar with one for D75H with ^{15}N-His(3). This result indicates that the cross-peaks with the splitting 0.6 MHz are produced by the N_ε of R71 that forms H-bond with SQ_H in D75H as well.

In contrast to the WT cyt *bo*$_3$, there are two histidines, i.e. H75 and H98, around the SQ_H in the D75H mutant. Experimental ^{14,15}N spectra do not give any indication which of them carries largest spin density on the N_ε atom. However, in our previous work we have provided arguments based on the comparison of the hyperfine couplings with methyl protons reflecting asymmetry in spin density distribution with the Q_A site SQ of the reaction center that stronger interaction with the N_ε of H75 is more preferable.[18] Taking into account this assignment one can conclude that the $\mathbf{N_{wc}}$ pattern in D75H with ^{15}N-His(3) includes contributions from N_δ of H75 and N_δ and N_ε of H98. The $\mathbf{N_{wc}}$ shoulders in this sample (Fig. 3B) show slight increase of intensity corresponding to the splitting ~0.8±0.2 MHz. We suggested that the N_ε from H98 forms the H-bond with the SQ_H similarly with the WT cyt *bo*$_3$ and produces this splitting. The N_δ s in H75 and H98 separated by two bonds from H-bonded N_εs would have much smaller couplings and would contribute to the central part of the N_{wc} line around the diagonal point. This suggestion is supported by about 1/20 ratio of the hyperfine couplings for the remote and coordinated imidazole nitrogens in complexes with metals and clusters.[32] We also suggested that N_αs from both His residues produce negligible influence on the spectra similarly as in the WT protein.

Hyperfine tensors of strongly coupled nitrogens

So far in our description of the experimental spectra we have used the hyperfine couplings determined from the position of cross-peak maxima using first-order expressions for two nuclear frequencies (Eqs.1, 2) of ^{15}N nuclei. However, the lineshape of the cross-peaks from strongly coupled nitrogens in the WT and D75H cyt *bo*$_3$ allows one to determine all of the principal values of hyperfine tensors. The cross-peaks from these nuclei possess the horn-like lineshape that indicates a significant rhombicity of the corresponding hyperfine tensors.[25,26] The principal values of the rhombic hyperfine tensor can be defined as follow: $A_x = a_{iso} - T(1 + \delta)$, $A_y = a_{iso} - T(1 - \delta)$, $A_z = a_{iso} + 2T$ with $0 \le \delta \le 1$, where a_{iso}, T are the isotropic and anisotropic components of hyperfine coupling and δ is a rhombic parameter. The two nuclear frequencies of ^{15}N (I = 1/2) from opposite $m_S = \pm½$ electron spin manifolds for each principal value i = x, y, z are $\nu_{\alpha i} = |^{15}\nu_N + |A_i|/2|$ and $\nu_{\beta i} = |^{15}\nu_N - |A_i|/2|$. An estimate of the principal components can be performed using theoretical predictions of the lineshape of the cross-peaks in powder-type spectra. The borders of the ideal cross-peak horn in such spectra are formed by three arc-type ridges between the pairs of three points ($\nu_{\alpha x}$, $\nu_{\beta x}$), ($\nu_{\alpha y}$, $\nu_{\beta y}$) and ($\nu_{\alpha z}$, $\nu_{\beta z}$) located on the $|\nu_1 \pm \nu_2| = 2(^{15}\nu_N)$ lines. The shape of these ridges is described by the general equation (where Q and G are coefficients which are functions of a_{iso},T, δ and $^{15}\nu_N$)[25,26]:

$$\nu_\alpha{}^2 = Q\nu_\beta{}^2 + G \quad (3)$$

The arc-type ridges transform to straight segments in $((\nu_1)^2$ *vs.* $(\nu_2)^2)$ plots, producing a triangle lineshape of the cross-peak with triangle vertexes at $((\nu_{\alpha(\beta)x})^2, (\nu_{\beta(\alpha)x})^2)$, $((\nu_{\alpha(\beta)y})^2, (\nu_{\beta(\alpha)y})^2)$, and $((\nu_{\alpha(\beta)z})^2, (\nu_{\beta(\alpha)z})^2)$.[25] It should be noted that HYSCORE intensity at $(\nu_{\alpha x}, \nu_{\beta x})$, $(\nu_{\alpha y}, \nu_{\beta y})$ and $(\nu_{\alpha z}, \nu_{\beta z})$ points corresponding to orientations of magnetic field along the principal directions (**x, y, z**) of the hyperfine tensor is equal to zero and significantly suppressed in the orientations around principal directions.[26] Therefore, in HYSCORE spectra only the central part of the border cross-ridges, which correspond to orientations of the magnetic field substantially different from the principal directions, will possess substantial intensity.[26] It means that in real spectrum the cross-peak borders should not cross the $|\nu_1 \pm \nu_2| = 2(^{15}\nu_N)$ line(s) and the crossing points $(\nu_{\alpha x}, \nu_{\beta x})$, $(\nu_{\alpha y}, \nu_{\beta y})$ and $(\nu_{\alpha z}, \nu_{\beta z})$ can be obtained through the linear regression of the observed parts of border arcs in $((\nu_1)^2$ *vs.* $(\nu_2)^2)$ presentation of the spectrum.

Fig. 4 (top) shows a presentation of the (++) quadrant of the ^{15}N HYSCORE spectrum of the SQ_H in WT cyt *bo*$_3$ in $((\nu_1)^2$ *vs.* $(\nu_2)^2)$ coordinates. The borders of the cross-peaks can be estimated by the area of the sharp increase of the peak intensity, i.e. where the blue background transformed into colored area in Fig. 4. In the spectrum shown in Fig. 4 **(bottom)**, only one border segment with a well-defined linear portion can be defined (pink line segment). Linear regression of this segment (pink line in Fig. 4, bottom) gives two crossing points $((\nu_{\beta x})^2, (\nu_{\alpha x})^2)$ and $((\nu_{\beta z})^2, (\nu_{\alpha z})^2)$, corresponding to the minimal and maximal principal values. The larger coordinate of the crossing points is estimated by the values 5.5–5.8 MHz^2 and 9.7–10.0 MHz^2 that defines ν_{ax} =2.3–2.4 MHz or $|A_x|$=1.7±0.1 MHz and ν_{az}=3.1–3.2 MHz or $|A_z|$=3.3±0.1 MHz, respectively. The intermediate principal value was determined from the simulations of ^{15}N HYSCORE spectra. Simulations varying the tensor anisotropy from axial (δ=1) to completely rhombic (δ=0) show that best agreement in the cross-peaks **1** location (Fig. S8) was achieved with δ=0.64±0.05, and defines the complete hyperfine tensor as $|A_z|$=3.3 MHz, $|A_y|$=2.3 MHz $|A_x|$=1.7 MHz (±0.1MHz) with a_{iso}=2.42 MHz and T=(0.88, −0.16, −0.72) MHz (signs a and T components are relative). All principal values A_i should have the same sign. Only this selection correctly describes the location of the cross-peak and gives the isotropic coupling consistent with the values estimated from ^{14}N and ^{15}N spectra. This tensor is assigned to the N_ε of R71. A similar analysis was performed for cross-peaks **1** in the (+−) quadrant of the ^{15}N HYSCORE spectrum of the SQ_H in the D75H mutant (see Figs. S9 and S10). Determined principal values of the hyperfine tensor assigned to the N_ε of H75 are shown in Table 2.

Hyperfine tensors of other nitrogens

In addition simulations of the ^{15}N HYSCORE spectra were used to estimate the isotropic and anisotropic components of the hyperfine tensors for weakly coupled nitrogens, i.e. N_η of R71 and N_ε of H98 in the WT cyt *bo*$_3$ and N_ε of H98 and N_ε of R71 in the D75H cyt *bo*$_3$. The results of simulations are provided in Table 2. The $\mathbf{N_{wc}}$ spectra are extended along antidiagonal of the (++) quadrant. They possess narrow linewidth in the direction normal to the antidiagonal and symmetrical line shapes with the cross-peak maximum corresponding to the undefined orientation of the magnetic field relative to the principal axes. The intensity is suppressed at the cross-peak wings corresponding to field orientations along or near the axes with maximum and minimum principal values of the tensor. Our previous analysis of the ^{15}N HYSCORE spectra[23] and simulations have shown that the position of the maximum gives accurate estimate of the isotropic coupling (~±0.05 MHz) but the relative signs of the isotropic and anisotropic components and symmetry of the tensor (i.e., axial or rhombic) are

uncertain from the $\mathbf{N_{WC}}$ lineshape. This uncertainty influences the accuracy in the anisotropic tensor estimate in larger degree, i.e. for T~0.3–0.4 MHz, and the accuracy in its determination is ~0.1–0.15 MHz.

Density Functional Studies

Previous modeling studies used water molecules and N-methylformamide groups as hydrogen bond donors to the O1 and O4 atoms of the SQ_H and did not take into account the varying strength of hydrogen bond interaction with the SQ_H by different groups.[33–35] In our work, based on the X-ray structure, Fig. 1, and the EPR and mutational data for the WT enzyme, the SQ_H was modeled to have hydrogen bonds to the OH of the carboxylic acid group of D75, the $N_\varepsilon H$ of the imidazole group of H98 and the $N_\varepsilon H$ group of the guanidium group of R71. In the absence of accurate data from the X-ray crystal structure, we explored idealized small models with geometry optimization. Therefore, the overall significance and relative strength of each interaction can be assessed by the spin density distribution, but the correct orientation of the hydrogen bonds with the SQ_H will not be well reproduced.

Computed Geometries

Table 3 shows the calculated geometry of the isolated SQ_H and the effect of hydrogen bonding on this geometry in the WT and D75H models. For the WT model, the hydrogen bond lengths of O1 with the R71 $N_\varepsilon H$ group (1.65 Å) and the D75 carboxylic acid group (1.60 Å) are considerably shorter than those formed at O4 with the imidazole NH representing H98 (1.83 Å). These bond distance trends suggest stronger hydrogen bonding to the O1 atom of the SQ_H caused principally by the strong interaction with the carboxylic acid group and the positively charged guanidium group. The NH group of the H98 imidazole is a weaker hydrogen bond donor. For the D75H model, the hydrogen bond length to the imidazole NH group from H75 is also significantly longer (1.79 Å) than that found for the carboxylic acid group of D75 in the WT model (1.60 Å) suggesting a weaker hydrogen bond formed by the imidazole group in the mutant.

Spin densities and populations

Fig. 5 shows the spin density distribution changes that occur on going from the isolated SQ to the WT and D75H models. Fig. 6 provides a more quantitative picture using spin populations obtained from a Mulliken population analysis. The spin density distribution of the isolated SQ is symmetric whereas, in contrast, it is highly asymmetric for both the WT and D75H. For simpler semiquinone models, the primary effect of hydrogen bonding to either of the semiquinone carbonyl oxygen atoms is a redistribution of spin density from the oxygen atom position to the adjacent carbon.[36] In our WT model (Fig. 6), the spin density redistribution is mainly from O1 to C1 with a much smaller redistribution occurring between C4 and O4. The charged guanidinum and carboxylic acid groups polarize the C1-O1 bond. The increased spin population at C1 leads via spin polarization to a lower spin population at positions C2 and C6 and a higher spin population at positions C3 and C5. This “domino” spin polarization effect should lead to a significantly lower spin population at C4, but this is offset by the presence of a hydrogen bond from the imidazole group of H98 to the O4 atom, which partially balances the spin polarization effect on C4. The spin populations obtained for WT can, therefore, be explained by the presence of strong hydrogen bonding to the O1 atom of the SQ_H and a significantly weaker hydrogen bond to the O4 atom, in accord with EPR studies. For the D75H model, the spin populations are slightly less asymmetric compared to the WT model. As noted above the hydrogen bond made by the imidazole is longer than that calculated for the carboxylic acid group suggesting a weaker hydrogen bond is formed by this group. The predicted spin density distributions are also in accord with the

lower 5-CH_3 ^{1}H and ^{13}C hyperfine couplings measured for the D75H mutant, as discussed below.

Comparison of calculated and experimental hyperfine couplings

In addition to the spin density distribution, hyperfine couplings can be calculated and compared with available ^{15}N, ^{1}H and ^{13}C experimental values. Table 4 shows the ^{15}N isotropic and anisotropic hyperfine couplings calculated for the WT and D75H models. In addition, the calculated ^{14}N qcc, K, and asymmetry parameters, η, are compared with experimental values. The experimental ^{15}N isotropic hyperfine couplings for the R71 N_ε and N_η (2.4 MHz and 0.15 MHz, respectively), as well as K (0.93 MHz) and η (0.51) for the R71 N_ε are excellently reproduced by the WT model. For the H98 imidazole NH, the calculations give a_{iso} = 0.4 MHz, in reasonable agreement with the experimental value of 0.3 MHz. The value of the isotropic hyperfine couplings for these nitrogens is very sensitive to the angle made by the NH donor with respect to the SQ ring plane.[37] The very close correspondence between calculated and experimental value for the WT model suggests that the orientation of these hydrogen bond donors in the optimized model is very similar to that adopted in the actual Q_H binding site.

For the D75H model, the optimized geometry gives rise to ^{15}N isotropic hyperfine couplings which deviate somewhat from the experimental determinations. The R71 N_ε has a calculated value of 1.4 MHz whereas the experimental assignment is 0.6 MHz. The calculated value for the N_εH group of H75 is 0.8 MHz whereas the experimental assignment is 3.5 MHz. For the H98 imidazole group, the calculated value, 0.6 MHz, is in good agreement with the experimental assignment of 0.8 MHz. In the optimized D75H model, the imidazole NH group is oriented 42° out of the SQ ring plane. The sensitivity of the ^{15}N value to this orientation is demonstrated by changing the orientation of the H75 NH group from the optimized value of 42° to 90°. This changes the calculated ^{15}N isotropic hyperfine coupling from 0.8 to 2.5 MHz, much closer to the experimentally measured 3.5 MHz. Likewise changing the out of plane orientation of the guanidium group N_εH from the optimized value of 41° to 35 ° changes the ^{15}N isotropic coupling from 1.4 MHz to 0.6 MHz in exact agreement with the experimental assignment. For the H75 imidazole NH group the calculated ^{14}N qcc K has a value of 0.5 MHz and the asymmetry parameter, η is calculated to be 0.6. These are in excellent agreement with our experimental determinations of 0.4 MHz and 0.7, respectively. Our conclusion, therefore, is that the D75H model is a good representation of the SQ_H in the mutant but the orientation of the hydrogen bond donors is different from the optimized small model calculation.

Calculated hyperfine couplings can also be compared with previous experimental determinations of ^{1}H hyperfine couplings for the WT and D75H mutant. Rotating methyl groups are observed readily using ENDOR spectroscopy as they give a strong ENDOR response and have been used as a primary marker in gauging the spin density asymmetry within SQs in photosynthetic reaction centers.[38] The 5-CH_3 ^{1}H hyperfine coupling has been measured in numerous studies and indeed is the principal indicator that the spin density of the WT SQ_H is highly asymmetric compared with the radical generated in vitro. For SQ in a non-polar solvent, and, therefore, not involved in hydrogen bonding, a_{iso} is 6.0 MHz.[38] Our calculated value for the isolated model is 5.9 MHz, which is in excellent quantitative agreement with this determination. For our WT model of SQ_H, the calculated ^{1}H a_{iso} value is 9.2 MHz, which is in good accord with experimental studies which vary from 9.5–10.0 MHz.[34] The elevated hyperfine coupling for the 5-CH_3 position is a result of the elevated spin population calculated for the ring C5 position shown in Fig. 6. Previous DFT studies[33–35] using SQ anion models have been unable to match the experimental value for this position and this can be mainly attributed to the use of water or amide groups as the hydrogen bonding groups in these modeling studies. Because the elevated 5-CH_3 hyperfine

coupling was similar to that found for neutral semiquinone free radicals, it has been proposed that the Q_H site SQ is a neutral radical.[17,18] No evidence for formation of the neutral SQ form has been obtained with the current computational model although this cannot be ruled out with a different larger model of the Q_H site. The asymmetry in spin density distribution for both scenarios is very similar. Our current computational studies indicate that the elevated 5-CH_3 coupling arises from strong hydrogen bonding of a semiquione anion radical to a positively charged guanidium group and a carboxylic acid group, i.e. R71 and D75 in the WT SQ_H.

For the D75H model, the calculated 5-CH_3 isotropic hyperfine coupling of 8.2 MHz is lower than that of the WT model and is in excellent agreement with the value found experimentally for the D75H mutant of 8.0 MHz.[18] The lower value for this hyperfine coupling, compared to the WT, can be ascribed to the more symmetric spin density distribution for the D75H model compared with the WT (Fig. 5 and 6). Replacement of the carboxylic acid group of D75 with the imidazole group of H75 results in significantly weaker hydrogen bonding to the O1 atom of SQ_H. The more symmetric spin density distribution leads to a lower spin density at C5 and a lower ^1H hyperfine coupling value for the 5-CH_3 group compared with the WT model. The good reproduction of this well characterized coupling suggests that the spin density distribution of the D75H model is reasonably accurate.

More recently, 2D ESEEM studies have obtained ^{13}C isotropic hyperfine coupling values for the 5-CH_3 carbon nucleus for both WT and D75H samples.[20] For the WT and D75H models, the calculated isotropic values −5.3 MHz and −4.4 MHz are in good agreement with the experimental values of −6.1 MHz and −4.7 MHz, respectively.

^1H hyperfine couplings have also been resolved from exchangeable, presumably hydrogen bonded, protons in both the WT and D75H mutant. Compared with methyl group hyperfine couplings, hydrogen bonded protons are difficult to interpret in complex systems where there can be significant overlap of spectral lines. For the WT SQ_H, 2D ESEEM identified three protons having isotropic and anisotropic values (a_{iso}, T) of (−/+ 0.7, ± 6.3) MHz; (−/+ 1.2, ±4.2) MHz; (−/+ 4.2, ±1.7) MHz.[17] The calculated values of (a_{iso}, $T=T_{11(max)}/2$) for the three hydrogen bonded protons from D75, R71 and H98 are, respectively: (0.0, 4.5) MHz, (−0.1, 4.3) MHz and (−0.6, 4.1) MHz (Table 5). The good agreement between the calculated R71N_ε, ^{15}N a_{iso}, value and experimental value indicates that the NH orientation relative to the SQ_H ring plane is accurately modeled for the WT. The most likely candidate for the strong H-bond observed experimentally is the COOH group of D75, which exhibits the shortest optimized hydrogen bonding distance. In the optimized model of the WT, this is oriented 40° out of the ring plane. By changing this orientation to 90° we calculate that the anisotropic coupling increases to 5.4 MHz with an isotropic coupling value of 0.8 MHz, which is in better agreement with the experimental values. Therefore, we assign the largest (−0.7, +6.3) MHz proton hyperfine coupling to the COOH proton of D75. The (−1.2, +4.2) MHz coupling could be due to an overlap of the H98 NH and R71 $N_\varepsilon H$ lines. None of our calculated values match the very unusual coupling of (−/+ 4.2, ±1.7) MHz. The unusually large isotropic coupling together with the relatively small anisotropic component would suggest that this coupling does not arise from a hydrogen bonded proton, and further experimental characterization is required.

For the D75H mutant exchangeable protons have been experimentally assigned to ^1H hyperfine couplings (a_{iso}, T) of (−/+ 1.0, ±4.6) MHz and (−/+ 4.3, ±1.2) MHz. Three hydrogen bond donors are present in our D75H model: R71 N_ε ^1H, H75 N^1H and H98 N^1H (Table 5). The calculated (a_{iso}, T) values of each of these are in reasonable agreement with the (1.0 MHz, +4.6 MHz) experimental value, so all three may contribute to this

experimentally determined coupling. As found with the WT model, the other experimentally observed coupling with a large isotropic and small anisotropic component, (−/+ 4.3, ±1.2) MHz, has no counterpart in the calculated values and is unlikely to be due to a proton(s) hydrogen bonded with carbonyls. One can suggest that exchangeable resonances with weaker *hfi* couplings observed in the spectra result from the overlap of the signals from the several protons in the SQ environment. Overlap of the cross-peak with different (but weak) hyperfine couplings would give cross-peaks with the shape and length substantially different from contributing signals. As the result the analysis would give some “effective” couplings not related directly to the real values. We suggest that further experiments using fully deuterated protein and cofactor as well as HYSCORE and ENDOR experiments at Q-band will better resolve these couplings, which would identify their source. Q-band will also address specific questions about the *orientation* of the H-bonds around the SQ_H site based on the hyperfine (and nuclear quadrupole) tensors of exchangeable protons (deuterons) that would lead to more adequate computational models.[39]

Relevance to quinone one-electron transfer role

For *in vitro* systems, in protic solvents, quinone reduction or quinol oxidation proceeds via sequential loss or gain of two electrons via the semiquinone free radical form with consequent loss or gain of two protons. In biological systems, quinones can function additionally as one-electron transfer agents. For example the Q_A-site quinone in Type II photosynthetic reaction centers acts as a one-electron transfer agent between a pheophytin molecule and the quinone reductase site Q_B.[28,38] In the Photostsystem I reaction center, a phylloquinone molecule, A_1, also acts as a one-electron transfer agent between a chlorophyll molecule and an Fe_4S_4 center.[40,41] For Q_B, which undergoes two electron reduction and subsequent protonation to the quinol, as in *in vitro* systems, a more symmetric spin density distribution is found.[38] The Q_B quinone is in dynamic equilibrium with a quinone pool and binds to receive two electrons and two protons before unbinding in the reduced quinol form. It is noteworthy that for the quinones functioning as one-electron transfer agents, an extremely asymmetric spin density distribution has been found for the SQ form, whereas in a true substrate binding quinone site, such as Q_B, a more symmetric spin density has been found i.e. similar to that found in protic solvents. To fulfill the role of a one-electron transfer agent it may be a requirement of the quinone binding site to produce a highly asymmetric spin density distribution for the SQ intermediate. The asymmetry in the spin density distribution for the semiquinone reflects a more contracted/localized electron density distribution for the singly occupied molecular orbital, SOMO, of the free radical anion. This is clearly shown by the spin density contours in Fig. 5. This contracted electron density distribution would be expected to lead to a less stable SQ form compared with the symmetrical form but would also imply that further one electron reduction to the two electron reduced dianion or quinol form would be unfavourable as now two electrons have to occupy the contracted asymmetric orbital. While the exact mechanism of electron transfer and reduction at the Q_H site is still unknown, it is believed to shuttle electrons from a true quinone substrate binding site Q_L to heme *b* for eventual reduction of oxygen at the heme o_3-Cu_B active site.[7,13] It would appear to perform a similar function as the Cu_A site in cytochrome *c* oxidase. As for the Q_A and A_1 quinones described above, the high asymmetry in spin density distribution observed for SQ_H, would indicate that it performs a similar one-electron transfer role and that high asymmetry in the SOMO electron density distribution may be a crucial factor in determining the quinone role as an effective one-electron transfer agent. In the present study therefore one possibility for the non-activity exhibited by the D75H mutant could be related to the more symmetrical spin density distribution of the Q_H site SQ compared with the WT. The asymmetry in spin density distribution is still quite large however for the D75H mutant, compared to the symmetrical situation. This would

argue against the above hypothesis, unless rapid one-electron transfer requires the extreme asymmetry which is present in the WT sample and also present in the Q_A and A_1 sites.

Conclusions

In this study, the pulsed EPR experiments performed with the selectively ^{15}N labeled cyt *bo*3 samples have led to the unambiguous assignment of the N_ε of R71 as the nitrogen that is strongly coupled to the Q_H-site SQ in the wild-type enzyme and gives rise to the observed ^{14}N ESEEM signals. In addition, selective ^{15}N labeling of cyt bo_3 has enabled the detection of even weak interactions between the SQ_H and individual residues at the ubiquinone binding site as summarized in Table 2. The HYSCORE data suggest that H98 at the Q_H-site is weakly coupled to the semiquinone radical and there is no direct interaction between the SQ_H and the N_ε of Q101. The ^{15}N selective labeling has also identified the N_ε of H75 as the nitrogen hydrogen bonded with the SQ_H of the D75H mutant enzyme.

Density functional calculations on models of the active site for both the WT and D75H systems show good agreement between for experimentally observed and calculated values of available $^{14,15}N$, ^{1}H and ^{13}C couplings. The model studies indicate that a very strong hydrogen bonding interaction occurs between the O1 atom of the SQ_H and the hydrogen bond donor groups of R71 and D75 with a relatively weaker interaction occurring for O4 and the imidazole NH group of H98. This is mainly responsible for the highly asymmetric spin density distribution observed experimentally. Replacement of D75 by H75 in the D75H mutant model leads to a lower spin density asymmetry for the SQ_H. The HYSCORE results also imply that in the D75H mutant, the $N_\varepsilon$of R71 possesses significantly smaller hyperfine coupling than that in the WT protein despite practically the same length of H-O bond in optimized structure. This suggests that the orientation of the hydrogen bond donors is different from the optimized small model calculation for D75H. Based on previous studies of quinone one-electron transfer sites, we further postulate that the highly asymmetric spin density distribution of the WT SQ_H may be a significant factor in its role as a one-electron transfer agent between the substrate binding site and heme *b*.

Overall, the combined pulsed EPR experiments and electronic structure calculations carried out in this study constitute a major step towards complete characterization of the distribution of the unpaired spin density of the SQ in the Q_H site. The interactions between the SQ and nearby residues unraveled in this study are crucial to understand how the radical is stabilized inside the protein's binding pocket and establish a foundation for future studies of quinone structure-function relationships in bioenergetics.

Supplementary Material

Refer to Web version on PubMed Central for supplementary material.

Acknowledgments

PJOM acknowledges the use of the EPSRC UK National Service for Computational Chemistry Software (NSCCS) in carrying out this work.

Abbreviations

2D	two-dimensional
CW EPR	continuous wave electron paramagnetic resonance
cyt *bo*$_3$	cytochrome bo_3 ubiquinol oxidase from *E. coli*

DDM	n-dodecyl-β-D-maltoside
DFT	Density Functional Theory
ESEEM	electron spin echo envelope modulation
HYSCORE	hyperfine sublevel correlation
nqi	nuclear quadrupole interactions
N_{wc}	weakly coupled nitrogens
qcc	quadrupole coupling constant
Q_H	the high affinity quinone-binding site
Q_L	the low affinity quinone-binding site
SQ	semiquinone
SQ_H	semiquinone at the Q_H site
UQ_8	ubiquinone-8
WT	wild-type

REFERENCES

1. Anraku Y. Bacterial electron transport chains. Annu. Rev. Biochem. 1988; 57:101–132. [PubMed: 3052268]
2. Puustinen A, Finel M, Virkki M, Wikstrom M. Cytochrome o (bo) is a proton pump in *Paracoccus denitrificans* and *Escherichia coli*. FEBS Lett. 1989; 249:163–167. [PubMed: 2544445]
3. Puustinen A, Finel M, Haltia T, Gennis RB, Wikstrom M. Properties of the two terminal oxidases of *Escherichia coli*. Biochemistry. 1991; 30:3936–3942. [PubMed: 1850294]
4. Garcia-Horsman JA, Barquera B, Rumbley J, Ma J, Gennis RB. The superfamily of heme-copper respiratory oxidases. J. Bacteriol. 1994; 176:5587–5600. [PubMed: 8083153]
5. Trumpower BL, Gennis RB. Energy transduction by cytochrome complexes in mitochondrial and bacterial respiration: The enzymology of coupling electron transfer reactions to transmembrane proton translocation. Annu. Rev. Biochem. 1994; 63:675–716. [PubMed: 7979252]
6. Puustinen A, Verkhovsky MI, Morgan JE, Belevich NP, Wikstrom M. Reaction of the *Escherichia coli* quinol oxidase cytochrome bo_3 with dioxygen: The Role of a bound ubiquinone molecule. Proc. Natl. Acad. Sci. U. S. A. 1996; 93:1545–1548. [PubMed: 8643669]
7. Yap LL, Lin MT, Ouyang H, Samoilova RI, Dikanov SA, Gennis RB. The quinone-binding sites of the cytochrome bo_3 ubiquinol oxidase from *Escherichia coli*. Biochim. Biophys. Acta. 2010; 1797:1924–1932. [PubMed: 20416270]
8. Sato-Watanabe M, Mogi T, Ogura T, Kitagawa T, Miyoshi H, Iwamura H, Anraku Y. Identification of a novel quinone-binding site in the cytochrome *bo* complex from *Escherichia coli*. J. Biol. Chem. 1994; 269:28908–28912. [PubMed: 7961852]
9. Sato-Watanabe M, Itoh S, Mogi T, Matsuura K, Miyoshi H, Anraku Y. Stabilization of a semiquinone radical at the high-affinity quinone-binding site (Q_H) of the *Escherichia coli bo*-type ubiquinol oxidase. FEBS Lett. 1995; 374:265–269. [PubMed: 7589550]
10. Ingledew WJ, Ohnishi T, Salerno JC. Studies on a stabilisation of ubisemiquinone by *Escherichia coli* quinol oxidase, cytochrome *bo*. Eur. J. Biochem. 1995; 227:903–908. [PubMed: 7867653]
11. Sato-Watanabe M, Mogi T, Miyoshi H, Anraku Y. Characterization and functional role of the Q_H site of *bo*-type ubiquinol oxidase from *Escherichia coli*. Biochemistry. 1998; 37:5356–5361. [PubMed: 9548917]
12. Mogi T, Sato-Watanabe M, Miyoshi H, Orii Y. Role of a bound ubiquinone on reactions of the *Escherichia coli* cytochrome *bo* with ubiquinol and dioxygen. FEBS Lett. 1999; 457:223–226. [PubMed: 10471783]

13. Kobayashi K, Tagawa S, Mogi T. Transient formation of ubisemiquinone radical and subsequent electron transfer process in the *Escherichia coli* cytochrome *bo*. Biochemistry. 2000; 39:15620–15625. [PubMed: 11112550]
14. Abramson J, Riistama S, Larsson G, Jasaitis A, Svensson-Ek M, Laakkonen L, Puustinen A, Iwata S, Wikstrom M. The structure of the ubiquinol oxidase from *Escherichia coli* and its ubiquinone binding site. Nat. Struct. Biol. 2000; 7:910–917. [PubMed: 11017202]
15. Hellwig P, Yano T, Ohnishi T, Gennis RB. Identification of the residues involved in stabilization of the semiquinone radical in the high-affinity ubiquinone binding site in cytochrome bo_3 from *Escherichia coli* by site-directed mutagenesis and EPR spectroscopy. Biochemistry. 2002; 41:10675–10679. [PubMed: 12186553]
16. Grimaldi S, MacMillan F, Ostermann T, Ludwig B, Michel H, Prisner T. Q_H^{*-} ubisemiquinone radical in the bo_3-type ubiquinol oxidase studied by pulsed electron paramagnetic resonance and hyperfine sublevel correlation spectroscopy. Biochemistry. 2001; 40:1037–1043. [PubMed: 11170426]
17. Yap LL, Samoilova RI, Gennis RB, Dikanov SA. Characterization of the exchangeable protons in the immediate vicinity of the semiquinone radical at the Q_H site of the cytochrome bo_3 from *Escherichia coli*. J. Biol. Chem. 2006; 281:16879–16887. [PubMed: 16624801]
18. Yap LL, Samoilova RI, Gennis RB, Dikanov SA. Characterization of mutants that change the hydrogen bonding of the semiquinone radical at the Q_H site of the cytochrome bo_3 from *Escherichia coli*. J. Biol. Chem. 2007; 282:8777–8785. [PubMed: 17267395]
19. Lin MT, Samoilova RI, Gennis RB, Dikanov SA. Identification of the nitrogen donor hydrogen bonded with the semiquinone at the Q_H site of the cytochrome bo_3 from *Escherichia coli*. J. Am. Chem. Soc. 2008; 130:15768–15769. [PubMed: 18983149]
20. Lin MT, Shubin AA, Samoilova RI, Narasimhulu KV, Baldansuren A, Gennis RB, Dikanov SA. Exploring by pulsed EPR the electronic structure of ubisemiquinone bound at the Q_H site of cytochrome bo_3 from *Escherichia coli* with in vivo ^{13}C-labeled methyl and methoxy substituents. J. Biol. Chem. 2011; 286:10105–10114. [PubMed: 21247900]
21. Datsenko KA, Wanner BL. One-step inactivation of chromosomal genes in *Escherichia coli* K-12 using PCR products. Proc. Natl. Acad. Sci. U. S. A. 2000; 97:6640–6645. [PubMed: 10829079]
22. Epel B, Silakov A. KAZAN viewer for Matlab™: Visualisation and data processing GUI for EPR and NMR. http://www.boep.specman4epr.com/kv_intro.html.
23. Martin E, Samoilova RI, Narasimhulu KV, Wraight CA, Dikanov SA. Hydrogen bonds between nitrogen donors and the semiquinone in the Q_B site of bacterial reaction centers. J. Am. Chem. Soc. 2010; 132:11671–11677. [PubMed: 20672818]
24. Höfer P, Grupp A, Nebenführ H, Mehring M. Hyperfine sublevel correlation (hyscore) spectroscopy: a 2D ESR investigation of the squaric acid radical. Chem. Phys. Lett. 1986; 132:279–282.
25. Dikanov SA, Bowman MK. Cross-peak lineshape of two-dimensional ESEEM spectra in disordered S = 1/2, I = 1/2 spin systems. J. Magn. Reson. A. 1995; 116:125–128.
26. Dikanov SA, Tyryshkin AM, Bowman MK. Intensity of cross-peaks in HYSCORE spectra of S = 1/2, I = 1/2 spin systems. J. Magn. Reson. 2000; 144:228–242. [PubMed: 10828191]
27. Frisch, MJ., et al. Wallingford CT: Gaussian, Inc.; 2009.
28. Lin T-J, O'Malley PJ. An ONIOM study of the spin density distribution of the Q_A site plastosemiquinone in the photosystem II reaction center. J. Phys. Chem. B. 2011; 115:4227–4233. [PubMed: 21428296]
29. Martin E, Samoilova RI, Narasimhulu KV, Lin TJ, O'Malley PJ, Wraight CA, Dikanov SA. Hydrogen bonding and spin density distribution in the Q_B semiquinone of bacterial reaction centers and comparison with the Q_A site. J. Am. Chem. Soc. 2011; 133:5525–5537. [PubMed: 21417328]
30. Dikanov SA, Samoilova RI, Kappl R, Crofts AR, Hüttermann J. The reduced [2Fe-2S] clusters in adrenodoxin and *Arthrospira platensis* ferredoxin share spin density with protein nitrogens, probed using 2D ESEEM. Phys. Chem. Chem. Phys. 2009; 11:6807–6819. [PubMed: 19639155]
31. Dikanov SA, Shubin AA, Kounosu A, Iwasaki T, Samoilova RI. A comparative, two-dimensional ^{14}N ESEEM characterization of reduced [2Fe-2S] clusters in hyperthermophilic archaeal high-

and low-potential Rieske-type proteins. J Biol. Inorg. Chem. 2004; 9:753–767. [PubMed: 15243789]

32. Iwasaki T, Kounosu A, Uzawa T, Samoilova RI, Dikanov SA. Orientation-selected ^{15}N-HYSCORE detection of weakly coupled nitrogens around the archaeal Rieske [2Fe−2S] center. J. Am. Chem. Soc. 2004; 126:13902–13903. [PubMed: 15506733]
33. Boesch SE, Wheeler RA. Isotropic ^{13}C hyperfine coupling constants distinguish neutral from anionic ubiquinone-derived radicals. Chem. Phys. Chem. 2009; 10:3187–3189. [PubMed: 19904797]
34. Kacprzak S, Kaupp M, MacMillan F. Protein–cofactor interactions and EPR parameters for the Q_H quinone binding site of quinol oxidase. A density functional study. J. Am. Chem. Soc. 2006; 128:5659–5671. [PubMed: 16637632]
35. MacMillan F, Kacprzak S, Hellwig P, Grimaldi S, Michel H, Kaupp M. Elucidating mechanisms in haem copper oxidases: The high-affinity Q_H binding site in quinol oxidase as studied by DONUT-HYSCORE spectroscopy and density functional theory. Faraday Discuss. 2011; 148:315–344. [PubMed: 21322491]
36. O'Malley PJ. Effect of hydrogen bonding on the spin density distribution and hyperfine couplings of the p-benzosemiquinone anion radical in alcohol solvents: A hybrid density functional study. J. Phys. Chem. A. 1997; 101:9813–9817.
37. O'Malley PJ. A density functional study of the effect of orientation of hydrogen bond donation on the hyperfine couplings of benzosemiquinones: relevance to semiquinone-protein hydrogen bonding interactions in vivo. Chem. Phys. Lett. 1998; 291:367–374.
38. Lubitz W, Feher G. The primary and secondary accepters in bacterial photosynthesis III. Characterization of the quinone radicals $Q_A^{-\cdot}$ and $Q_B^{-\cdot}$ by EPR and ENDOR. Appl. Magn. Reson. 1999; 17:1–48.
39. Flores M, Isaacson R, Abresch E, Calvo R, Lubitz W, Feher G. Protein-cofactor interactions in bacterial reaction centers from Rhodobacter sphaeroides R-26: II. Geometry of the hydrogen bonds to the primary quinone $Q^{\cdot}{}_A^-$ by ^{1}H and ^{2}H ENDOR spectroscopy. Biophys. J. 2007; 92:671–682. [PubMed: 17071655]
40. Lin T-J, O'Malley PJ. Binding site influence on the electronic structure and electron paramagnetic resonance properties of the phyllosemiquinone free radical of photosystem I. J. Phys. Chem. B. 2011; 115:9311–9319. [PubMed: 21662975]
41. Srinivasan N, Golbeck JH. Protein-cofactor interactions in bioenergetic complexes: The role of the A_{1A} and A_{1B} phylloquinones in Photosystem I. Biochim. Biophys. Acta. 2009; 1787:1057–1088. [PubMed: 19409369]

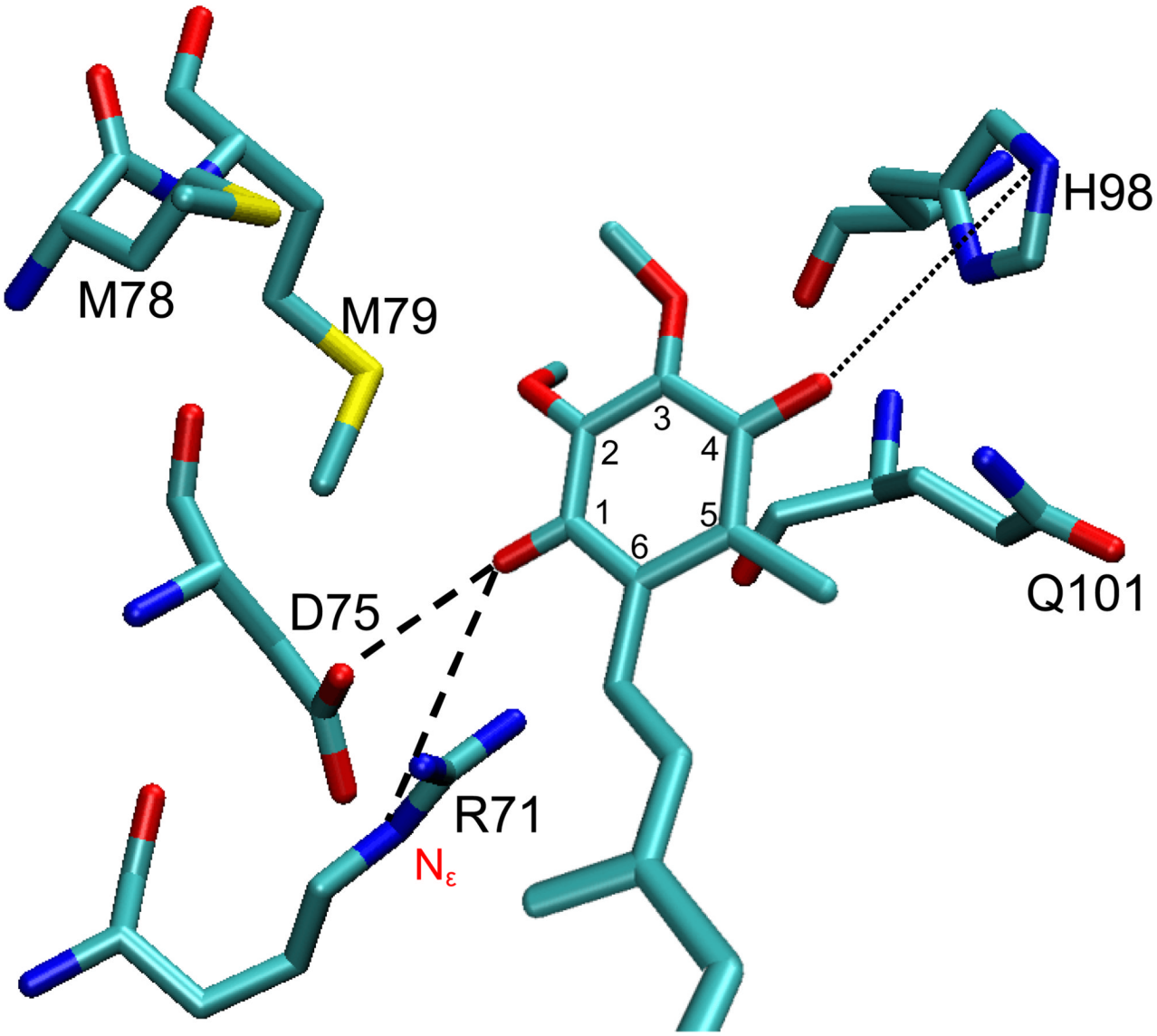

Figure 1.
The current model of UQ at Q_H site of cyt *bo*$_3$. The strong H-bonds are shown in dashed lines and the weak one in a dotted line. The figure was generated according to the model based on the X-ray crystal structure by Abramson et al.[14] Adapted from ref. (20).

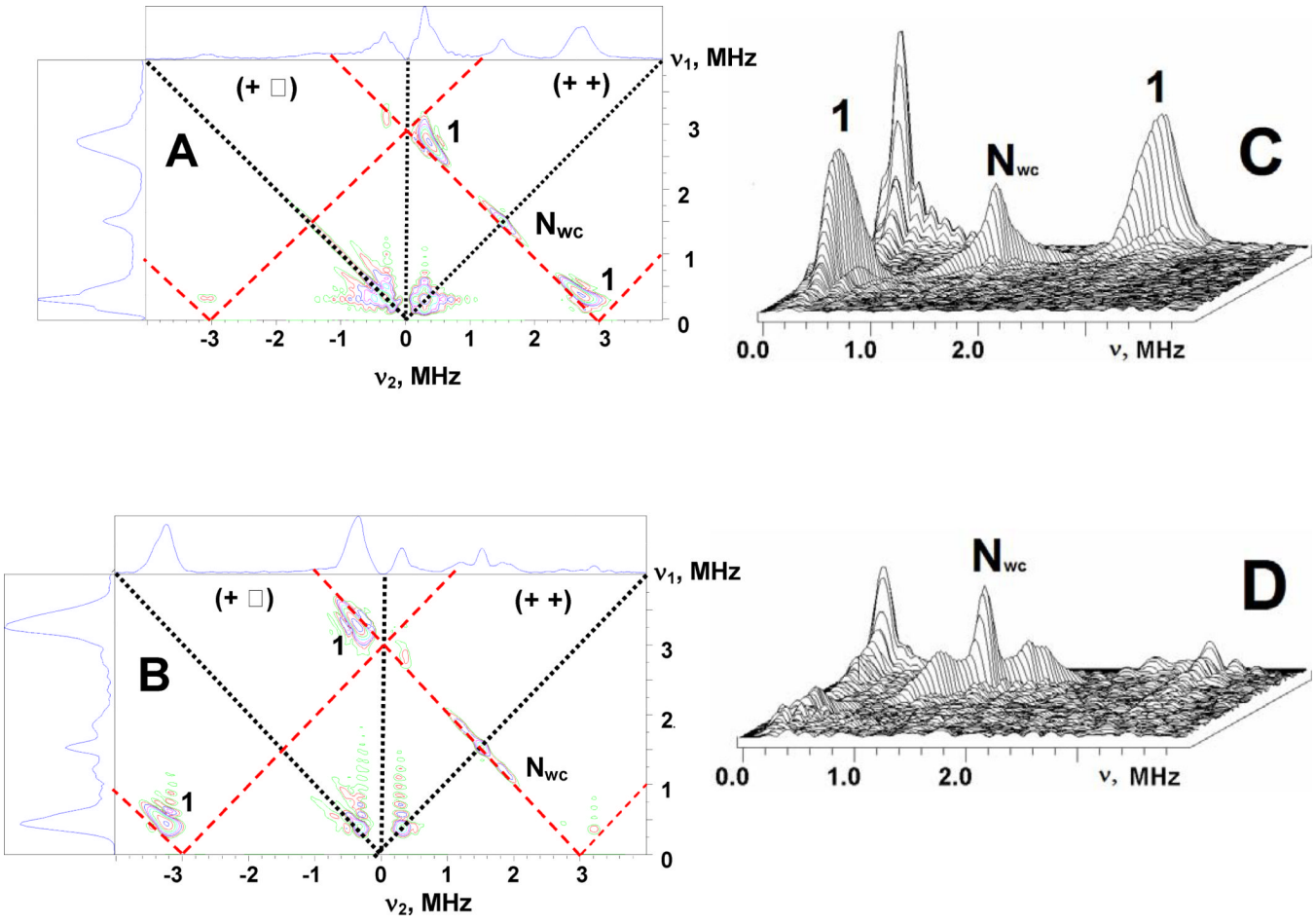

Figure 2.

Contour (A,B) presentation of the ^{15}N HYSCORE spectra of the SQ_H in ^{15}N uniformly labeled WT (A) and D75H (B) cyt bo_3 (magnetic field 345.2 mT (A) and 346.1 mT (B), time between first and second pulses τ=136 ns, microwave frequency 9.702 GHz (A) and 9.704 GHz (B)). Stacked (C,D) presentation of the (++) quadrant of the WT (C) and D75H (D) spectra. Stacked presentation of the full (A) and (B) spectra is shown in Figure S4. Red dashed straight segments are defined by $|\nu_1 \pm \nu_2| = 2(^{15}\nu_N)$.

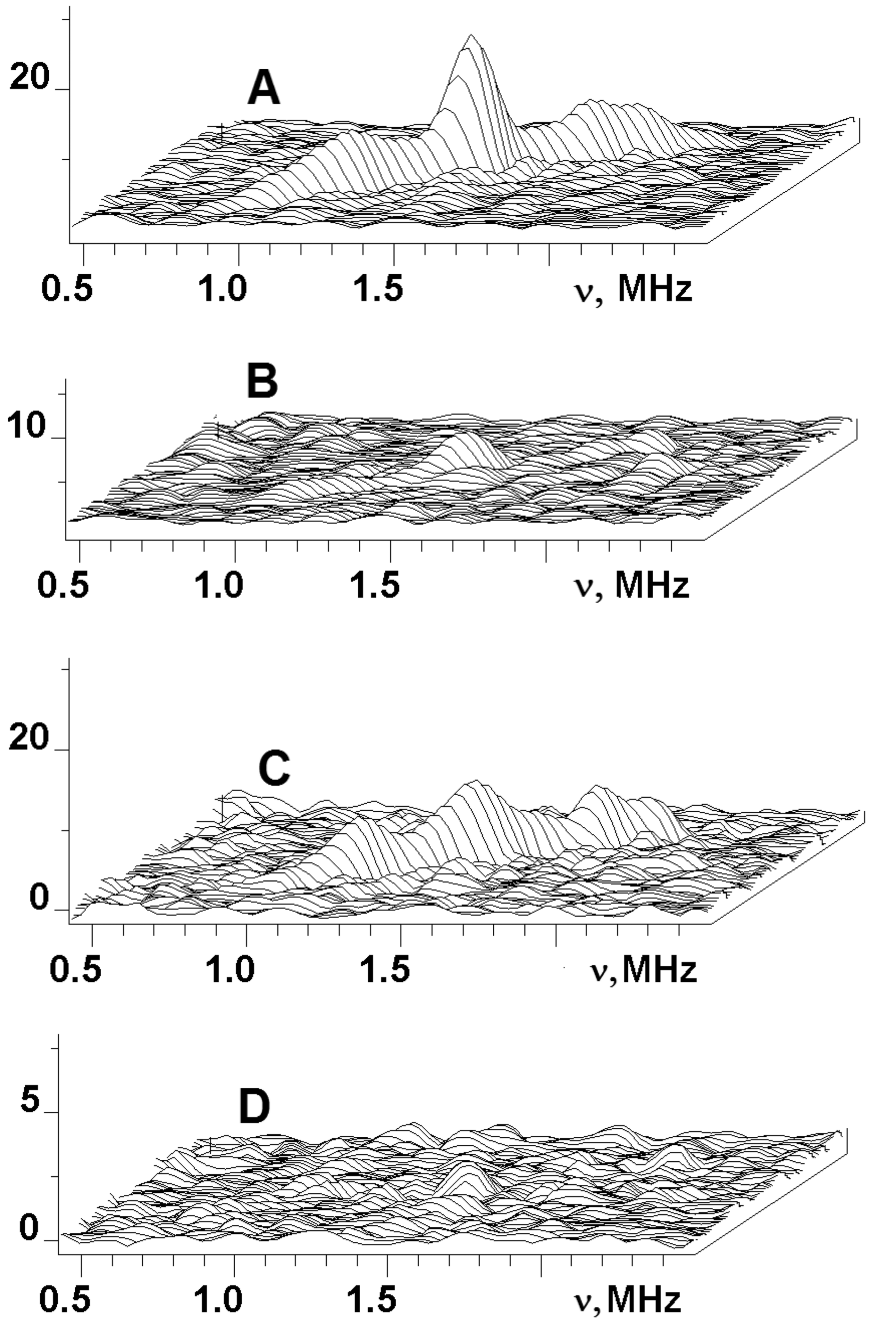

Figure 3.

$\mathbf{N_{wc}}$ feature in ^{15}N HYSCORE spectra of SQ_H in ^{15}N -U D75H (A), D75H with uniformly ^{15}N(3) labeled His (B), (C) obtained as a difference between the spectra of ^{15}N -U D75H and ^{15}N-U D75H except Arg, (D) obtained as a difference between the spectra of ^{15}N-U D75H except Arg and D75H with uniformly ^{15}N(3) labeled His.

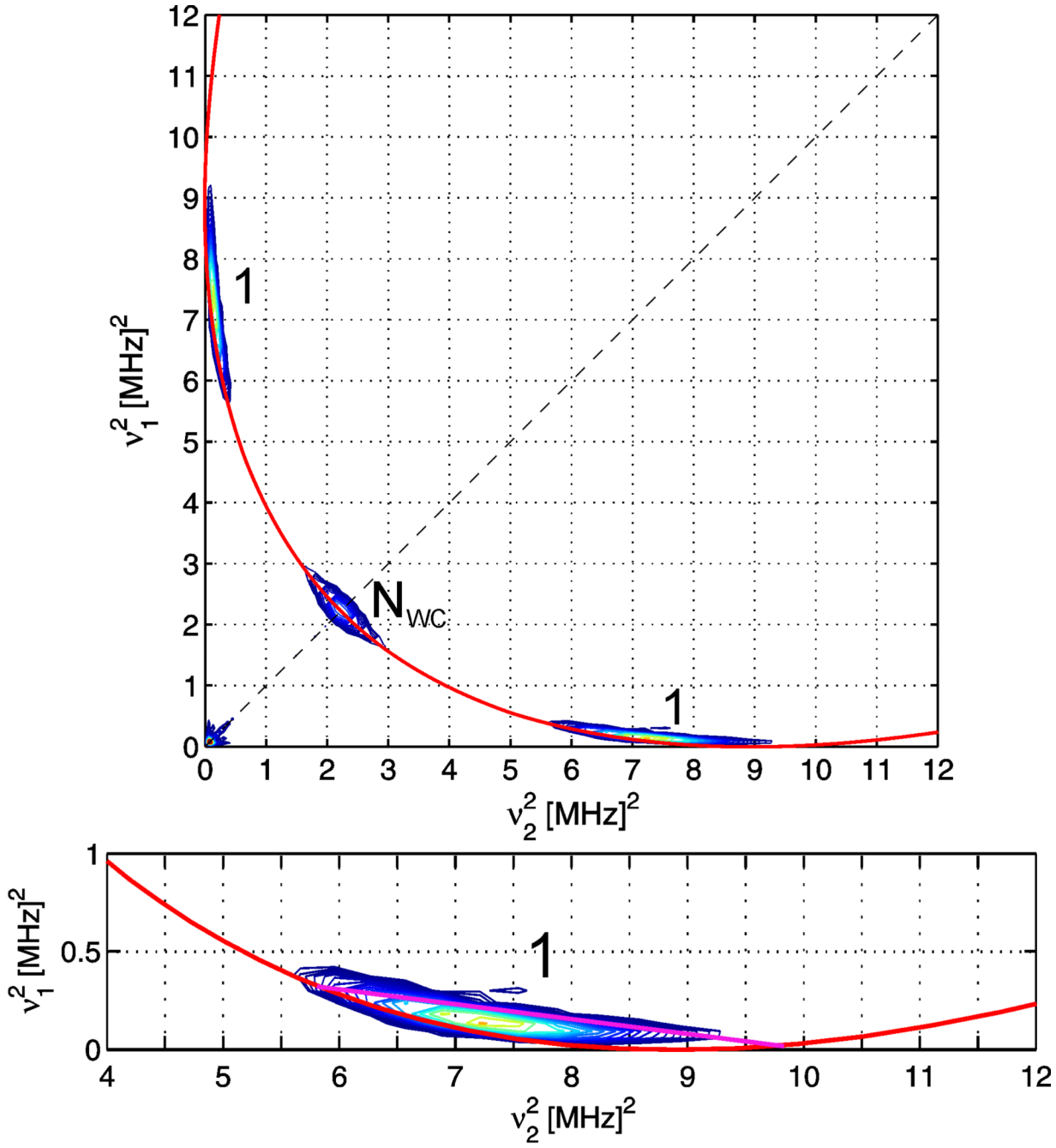

Figure 4.

(top) Contour presentation of the (++) quadrant from the ^{15}N HYSCORE spectrum of the SQ_H in ^{15}N uniformly labeled WT cyt *bo*$_3$ (Fig.2A) in $((\nu_1)^2$ vs. $(\nu_2)^2)$ coordinates. The red curve is defined by $|\nu_1 \pm \nu_2| = 2(^{15}\nu_N)$.

(bottom) Analysis of the cross-peak **1** contour lineshape. Linear regression of the border segment (pink line) gives two crossing points $((\nu_{\beta x})^2, (\nu_{\alpha x})^2)$ and $((\nu_{\beta z})^2, (\nu_{\alpha z})^2)$ with $|\nu_1 \pm \nu_2| = 2(^{15}\nu_N)$ curve corresponding to minimum and maximum principal values of hyperfine tensor.

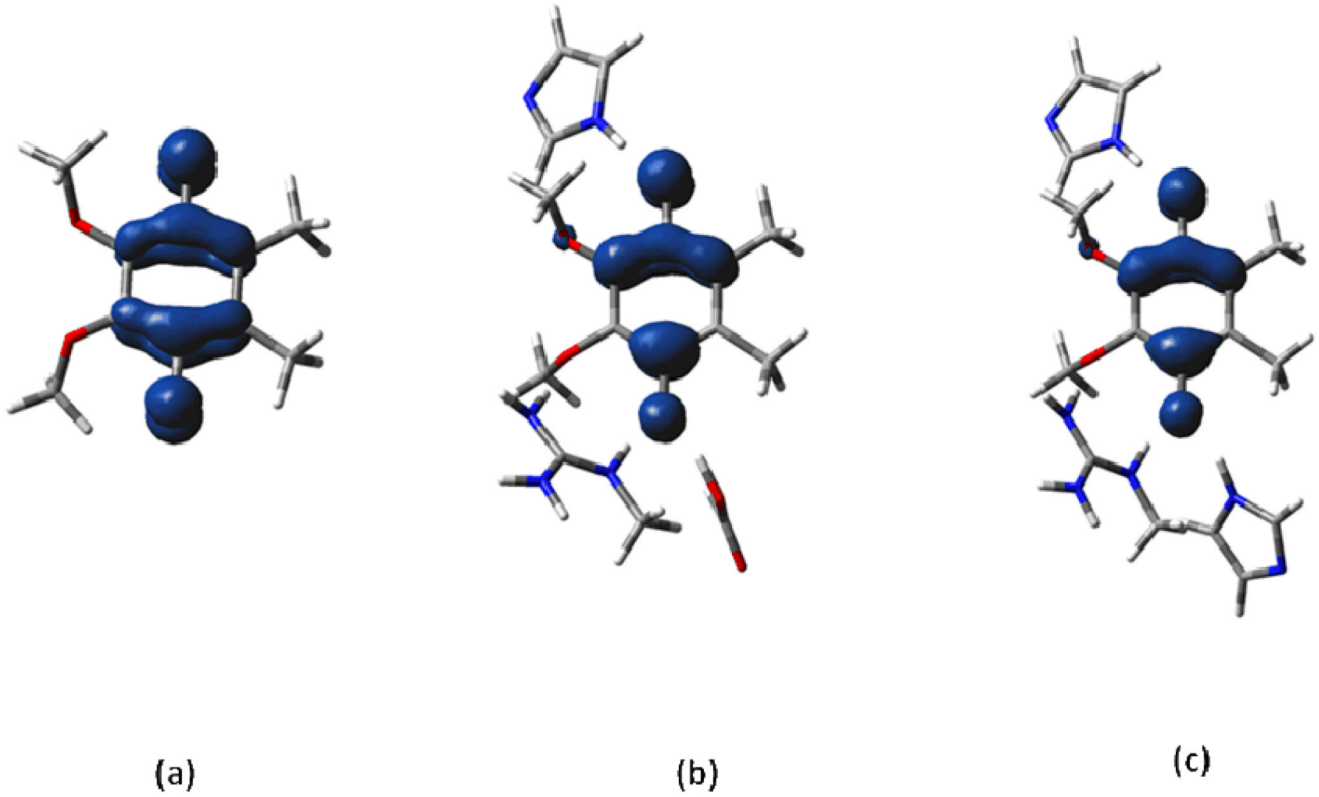

Figure 5.
Spin density contour plots (0.004e/au) for (a) Isolated, (b) WT and (c) D75H models. Atom numbering is as shown in Fig. 1.

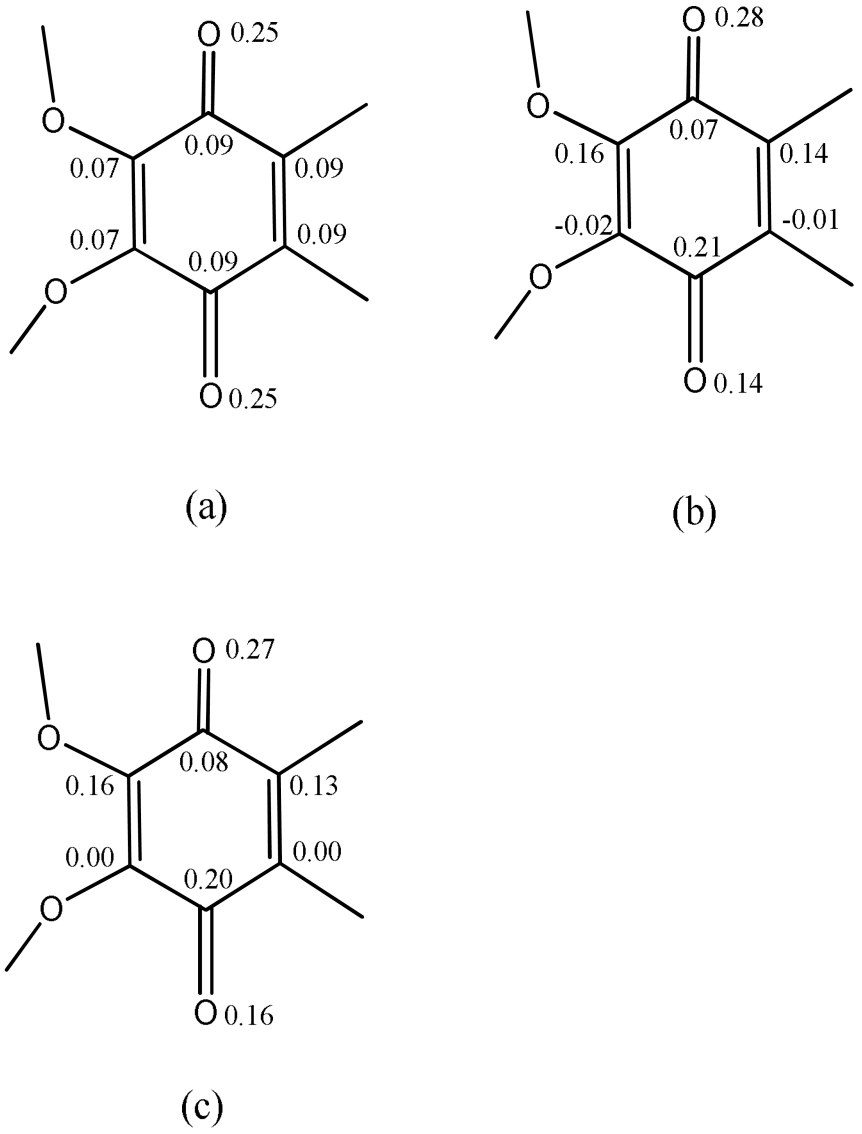

Figure 6.
Mulliken spin populations for (a) Isolated, (b) WT and (c) D75H models. Atom numbering is as shown in Fig. 1.

Table 1

The genotype of *E. coli* C43(DE3) auxotrophs used for the preparation of selectively ^{15}N labeled cyt bo_3 samples and amino acids supplemented to the minimal medium to grow these auxotrophs.

***E. coli* C43(DE3) strains**	**Genes knocked out**	**Amino acids added to the minimal medium**	**Cyt bo_3 samples prepared**	
C43(DE3)	none	none	**1**	Uniformly ^{15}N labeled WT cyo bo_3
CLY	*cyo*	none	**1**	Uniformly ^{15}N labeled D75H cyo bo_3
ML8	*cyo, argH*	105 mg/L Arg	**1**	WT cyt bo_3 with $^{15}N_\eta$ Arg
			2	WT cyt bo_3 with $^{15}N_\alpha$ Arg
			3	WT cyt bo_3 with $^{15}N_4$ Arg
			4	D75H cyt bo_3 with uniform ^{15}N except for Arg
			5	D75H cyt bo_3 with uniform ^{15}N except for the N_ε and N_α of Arg
ML17	*glnA*	750 mg/L Gln	**1**	WT cyt bo_3 with $^{15}N_\varepsilon$ Gln
ML21	*tyrA, hisG*	18 mg/L Tyr, 15 mg/L His	**1**	WT cyt bo_3 with $^{15}N_3$ His
			2	WT cyt bo_3 with $^{15}N_\delta$ His
ML22	*cyo, ilvE, avtA, aspC, hisG*	40 mg/L Ile, 40 mg/L Leu, 35 mg/L Val, 90 mg/L Tyr, 50 mg/L Phe, 40 mg/L Asp, 16 mg/L His	**1**	WT cyt bo_3 with ring $^{15}N_2$ His
			2	D75H cyt bo_3 with $^{15}N_3$ His
			3	D75H cyt bo_3 with $^{15}N_\delta$ His
ML26	*cyo, ilvE, avtA, aspC, hisG, argH*	40 mg/L Ile, 40 mg/L Leu, 35 mg/L Val, 90 mg/L Tyr, 50 mg/L Phe, 40 mg/L Asp, 16 mg/L His, 105 mg/L Arg	**1**	D75H cyt bo_3 with $^{15}N_4$ Arg
ML30	*cyo, ilvE, avtA, aspC, hisG, argH, glnA*	40 mg/L Ile, 40 mg/L Leu, 35 mg/L Val, 90 mg/L Tyr, 50 mg/L Phe, 40 mg/L Asp, 16 mg/L His, 105 mg/L Arg, 750 mg/L Gln	**1**	D75H cyt bo_3 with $^{15}N_\varepsilon$ Gln
ML32	*cyo, argH, glnA*	105 mg/L Arg, 750 mg/L Gln	**1**	D75H cyt bo_3 with uniform ^{15}N except for Arg and Gln
ML34	*cyo, argH, glnA, hisG*	105 mg/L Arg, 750 mg/L Gln, 16 mg/L His	**1**	WT cyt bo_3 with uniform ^{15}N except for Arg, Gln and His

Table 2

Hyperfine tensors of ^{15}N nuclei at the Q_H-site of cyt *bo*$_3$ proteins.

Cytochrome *bo*$_3$	Residue	Nitrogen	Hyperfine tensors (MHz)
Wild-type	R71	N_ε N_η N_α	a_{iso}=2.42, ***T***=(0.88, −0.16, −0.72) a_{iso} ~0.15, T<0.05–0.1 ~0
	H98	N_δ N_ε N_α	~0 a_{iso}=0.3, T~0.3–0.4 ~0
	Q101	N_ε	Weak dipolar coupling <0.05–0.1 MHz
D75H	H75	N_ε	a_{iso}=3.5, ***T***= (0.9, −0.2, −0.7)
	H98	N_ε N_δ	a_{iso}=0.8, $\|T\|$~ 0.3–0.4
	R71	N_ε N_η	a_{iso}=0.6, $\|T\|$~ 0.4–0.5 ~0
	Q101	N_ε	Weak dipolar coupling <0.05–0.1 MHz

Table 3

Optimised geometries. All distances in angstroms.

	Isolated	WT	D75H
C1-O1	1.27	1.30	1.30
C4-O4	1.27	1.27	1.27
O1-H (R71)	-	1.65	1.61
O1-H (D75/H75)	-	1.60	1.79
O4-H (H98)	-	1.83	1.82

Table 4

^{15}N isotropic, a_{iso}, and anisotropic, T_{ii}, hyperfine tensors calculated for the Q_H site models. Calculated values for the ^{14}N Nuclear Quadrupole Coupling Constant (K) and the asymmetry parameter, η are also given. Experimental values are given in brackets. All values given in MHz.

	WT Model				D75H			
Pos.	**$T_{zz}T_{yy}T_{xx}$**	**a_{iso}**	**K**	**η**	**$T_{zz}T_{yy}T_{xx}$**	**a_{iso}**	**K**	**η**
R71 - Nε	0.6(0.9) −0.3(−0.6) −0.3(0.3)	2.4 (2.4)	0.9 (0.9)	0.7 (0.5)	0.0 0.0 0.0	1.4, 0.5 * (0.6)	0.9	0.8
R71 - Nη	0.0 0.0 0.0	0.2 (0.15)	1.1	0.4	0.0 0.0 0.0	0.0 (0.0)	1.1	0.5
R71 - Nη	0.0 0.0 0.0	0.0	1.2	0.2	0.0 0.0 0.0	0.0 (0.0)	1.2	0.3
H98 - N	0.4 −0.1 −0.3	0.4 (0.3)	0.6	0.5	0.5 −0.2 −0.3	0.6 (0.8)	0.6	0.6
H75 - N	-	-	-	-	0.4, 0.7 *(0.9) −0.2,−0.4 *(−0.7) −0.2,−0.3 *(−0.2)	0.8, 2.5 * (3.5)	0.5(0.4)	0.6 (0.7)

* Values using adjusted orientation, see text for details.

Table 5

5-Methyl and Hydrogen bonded ^{1}H isotropic, a_{iso}, and anisotropic, T_{ii}, hyperfine tensors calculated for the Q_H site model. Experimental values are given in brackets. All values are given in MHz.

	Isolated		WT		D75H	
Pos.	$T_{zz}T_{yy}T_{xx}$	a_{iso}	$T_{zz}T_{yy}T_{xx}$	a_{iso}	$T_{zz}T_{yy}T_{xx}$	a_{iso}
5- CH3	2.6 −1.3 −1.3	5.9 (6.0)	3.0 −1.5 −1.5	9.2 (9.5–10.0)	2.7 −1.4 −1.4	8.2 (8.0)
R71 - NHε	-	-	8.6 −4.1 −4.5	−0.1	8.4 −4.1 −4.3	−0.2
R71 - NHη	-	-	1.8 −0.6 −1.2	0.0	1.8 −0.6 −1.2	0.0
R71 - NHη	-	-	0.8 −0.3 −0.5	0.0	0.8 −0.3 −0.5	0.0
H98 - NH	-	-	8.2 −3.9 −4.2	−0.6	8.3 −4.0 −4.3	−0.7
D75/H75 – COOH/NH	-	-	8.9 −4.4 −4.5	0.0	6.5 −3.2 −3.3	−0.4